

# End-to-end Temporal Action Detection with Transformer

Xiaolong Liu<sup>1\*</sup> Qimeng Wang<sup>1</sup> Yao Hu<sup>2</sup> Xu Tang<sup>2</sup> Song Bai<sup>1</sup> Xiang Bai<sup>1</sup>  
<sup>1</sup>Huazhong University of Science and Technology <sup>2</sup>Alibaba Group  
 {liuxl, qimengwang, xbai}@hust.edu.cn, songbai.site@gmail.com  
 {yaoohu, buhui.tx}@alibaba-inc.com

## Abstract

Temporal action detection (TAD) aims to determine the semantic label and the boundaries of every action instance in an untrimmed video. It is a fundamental and challenging task in video understanding and significant progress has been made. Previous methods involve multiple stages or networks and hand-designed rules or operations, which fall short in efficiency and flexibility. In this paper, we propose an end-to-end framework for TAD upon Transformer, termed TadTR, which maps a set of learnable embeddings to action instances in parallel. TadTR is able to adaptively extract temporal context information required for making action predictions, by selectively attending to a sparse set of snippets in a video. As a result, it simplifies the pipeline of TAD and requires lower computation cost than previous detectors, while preserving remarkable detection performance. TadTR achieves state-of-the-art performance on HACS Segments (+3.35% average mAP). As a single-network detector, TadTR runs 10× faster than its comparable competitor. It outperforms existing single-network detectors by a large margin on THUMOS14 (+5.0% average mAP) and ActivityNet (+7.53% average mAP). When combined with other detectors, it reports 54.1% mAP at IoU=0.5 on THUMOS14, and 34.55% average mAP on ActivityNet-1.3. Our code will be released at <https://github.com/xlliu7/TadTR>.

## 1. Introduction

Video understanding has become more important than ever as the rapid growth of media prompts the generation, sharing, and consumption of videos. As a fundamental task in video understanding, temporal action detection (TAD) aims to predict the semantic label, the start time, and the end time of every action instance in an untrimmed and possibly long video. For its wide range of applications, including security surveillance, home care, video editing, and so on,

\*Work done during an internship at Alibaba Group.

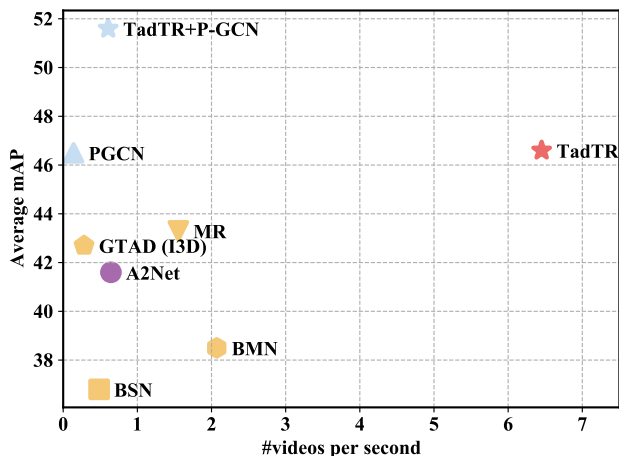


Figure 1. Comparison of recent temporal action detection methods on THUMOS14, in terms of both performance (average mAP) and speed. Our method state-of-the-art performance while running more than 3× faster. When combined with a two-stage method P-GCN [43], it achieves 51.6% average mAP, and is still faster than many of the compared methods.

temporal action detection has gained increasing attention from the community in recent years [31, 37, 25, 28, 4, 20].

Many previous TAD methods have complicated pipelines. As shown in Fig. 2, these pipelines involve multiple steps, such as segment scoring, proposal generation, action classification, and post-processing. While these methods achieve promising performance on standard benchmarks, there are several limitations. Firstly, the multiple steps may increase the time cost since they need to be carried out sequentially. Some stages, such as the proposal classification stage, are time-consuming when there is a large number of candidates ( $10^3 \sim 10^4$ ). Secondly, the hand-designed operations, such as anchor setting and ground truth assignment, restrict the flexibility of a method. Thirdly, they can not enjoy end-to-end training. For example, some multi-stage methods, such as BSN, BMN, and G-TAD, need to train at least two different networks to get action detection results. Although some

methods unify all steps in a single network, they require non-differentiable steps such as non-maximal suppression (NMS) and grouping. As a consequence, multiple stages may accumulate errors and lead to sub-optimal results.

In this paper, we propose a simple end-to-end temporal action detector. The detector adopts a set-prediction pipeline that directly maps a set of learnable embeddings to action instances in parallel. This is different from previous methods that achieve action detection by classifying pre-defined anchors or proposals. In these methods, it is straightforward to extract features in certain time intervals according to the locations of the anchors or proposals. The set-prediction pipeline, however, requires to extract sufficient temporal information before knowing which interval an action falls in. In other words, the network should learn where to look at when predicting actions. To do that, we design a Transformer architecture that adaptively extracts the temporal context required by each action prediction and updates the initial embeddings with the extracted context. The core is the temporal deformable attention module that dynamically attends to a sparse set of key snippets in the video, similar to the way human finds actions in a video. It is more flexible than previous works that extract context information by increasing the receptive field by a fixed ratio [9, 8]. Furthermore, it requires less computation cost than the vanilla self-attention module [33] that attends to all locations in an input sequence. Upon each embedding enhanced with video context, two feed-forward networks (FFNs) predict the class and the segment of the corresponding action prediction. To better rank the actions, an actionness regression head is attached to predict the actionness (confidence score, similar to objectness in object detection) of these action predictions from the context aligned with the corresponding segment. During training, a segment matching module dynamically determines a one-to-one ground truth assignment. Owing to this, our detector avoids duplicate detections and NMS is unnecessary. It produces a very sparse set of action detections ( $10 \sim 10^2$ ), orders of fewer than previous methods.

The temporal action detection Transformer, dubbed as TadTR, achieves remarkable performance with low computation cost. Without bells and whistles, TadTR achieves state-of-the-art performance on HACS Segments and THUMOS14. When combined with existing methods, it reaches 51.6% average mAP on THUMOS14 [15] and 34.55% average mAP on ActivityNet-1.3 [5], outperforming strong competitors such as G-TAD [37] and P-GCN [43]. In terms of efficiency, it takes only 155 ms per video with a single network, which is more than  $3 \times$  faster than recent state-of-the-art methods, as shown in Fig. 1.

The contributions of this work are three-fold:

- We propose an end-to-end set-prediction-based detector that simplifies the pipeline for temporal action de-

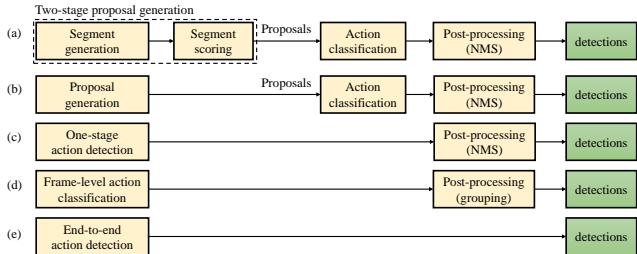


Figure 2. Comparison of different pipelines of temporal action detection. (a) Multi-stage pipeline in [31, 37] *etc.* (b) Two-stage pipeline in [36, 8]. (c) Top-down one-stage pipeline in [17], (d) Bottom-up one-stage pipeline in [42] (e) An end-to-end pipeline in this work.

tection.

- We propose a Transformer architecture that is able to adaptively capture temporal context for temporal action detection. To the best of our knowledge, this is the first work that explores adaptive context for TAD.
- Our method achieves state-of-the-art or highly competitive performance on standard datasets and requires lower computation cost than its competitors.

## 2. Related Works

### 2.1. Temporal Action Detection Methods

Previous methods for temporal action detection can be roughly categorized into groups depending on the pipeline.

(a) **Multi-stage methods** [37, 16, 41]. They first generate candidate segments and train a binary classifier that associates each segment with a confidence score, resulting in proposals. Those proposals with high scores are fed to a multi-class classifier to classify the actions. The candidate segments are generated by dense uniform sampling [31, 12] or grouping local frames that may contain actions [18]. Some methods [11, 21] combine multiple schemes for complementarity. (b) **Two-stage methods** [36, 8, 10, 3] simplify the multi-stage pipeline by adopting a one-stage proposal generator, which directly predicts the scores and boundaries of pre-defined multi-scale anchors associated with each temporal location. These methods need to manually set multiple anchor scales, which restricts the flexibility. (c) **Top-down one-stage methods** [17, 22] can be seen as the class-aware variant of the one-stage proposal generator. Recently, [38] augment the anchor-based one-stage detector with an anchor-free branch that makes predictions based on centers of actions. (d) A **bottom-up one-stage method** proposed in [42] first predicts the action and boundary probabilities and then groups frames with maximal structured sum as actions. We note that all the above methods require post-processing steps such as NMS or grouping, which prevent end-to-end learning.

An early work by [39] proposes an end-to-end temporal action detector based on recurrent neural networks (RNN) and reinforcement learning (RL). It learns action detection by training an agent that iteratively picking an observation location and deciding whether to emit or refine a candidate action after observation. In this work, an end-to-end Transformer-based detector significantly different from [39] is proposed. While [39] is restricted to a manner of one-by-one prediction due to the recurrent nature of RNN, our method can decode all action instances in parallel. In addition, our method is fully differentiable, whereas the RL-based method is not.

All the methods discussed above are fully supervised methods. There are also some weakly supervised methods [24, 19, 26, 27, 30, 34, 40], which are beyond the scope of this paper.

## 2.2. Transformers for Video Understanding

Transformers [33] have achieved great success in natural language processing. The core of Transformer is the self-attention mechanism that aggregates non-local cues through a weighted sum of features at attended locations. Compared with convolutions, self-attention can capture long-range context and dynamically adjust weights according to the input. Recently, many works have revealed the great potential of Transformers in video understanding tasks. For example, VideoBert [32] and ActBert [49] utilize Transformers to learn a joint representation for video and text. TimeS-former [2] decouples spatial and temporal self-attention for video classification. Zhou *et al.* [48] capture the temporal dependency with Transformer for video captioning. Girdhar *et al.* [13] apply Transformer to model the relationship between spatial proposals for spatio-temporal action detection.

In this paper, Transformer is used to capture temporal context information for temporal action detection. Specifically, We employ attention modules to model the relationship between video snippets, the relationship between actions and frames, and the relationship between actions. Different from many previous works where an attention module attends to all locations in the input sequence, we introduce a temporal deformable attention module that adaptively attends to a sparse set of key frames instead of all frames. Therefore, context information can be extracted without excessive computation cost. Besides adaptive context, we also employ an actionness regression head to extract aligned context in order to assign reliable confidence scores to the detections by Transformer.

## 3. TadTR

TadTR is constructed on video features encoded with a pre-trained video classification network (e.g. I3D [7]). Fig. 3 shows the overall architecture of TadTR. TadTR takes the

video features and the temporal position encoding as input and outputs a set of action predictions. It consists of a Transformer encoder to model the interactions between frames, a Transformer decoder to predict action segments, and an extra actionness regression head to estimate the confidence score of the predicted segments. A segment matching module is used for ground truth assignments during training.

### 3.1. Architecture

**Encoder.** Let  $X_V \in \mathbb{R}^{T_S \times C_V}$  denotes the video feature sequence, where  $T_S$  and  $C_V$  are the length and dimension, respectively. Each frame in the feature sequence is a feature vector extracted from a certain snippet in the video. Here, a snippet means a sequence of a few (e.g., 8) consecutive frames. A 1D convolutional layer with kernel size 1 is applied to reduce its dimension to  $C$ . The encoder models the relation between different snippets and outputs a feature sequence  $X_E \in \mathbb{R}^{T_S \times C}$  enhanced with temporal context. As depicted in Fig. 3, it consists of  $L_E$  Transformer encoder layers of the homogeneous architecture, where the key component is the attention module.

The primitive dense attention module in [33] attends to all locations in an input feature sequence, suffering from high computation cost and slow convergence. To mitigate these issues, we employ a temporal deformable attention (TDA) module that adaptively attends to a sparse set of temporal locations around a reference location in the feature sequence.

Let  $z_q \in \mathbb{R}^C$  be denote the feature of query  $q$  and  $t_q \in [0, 1]$  be the normalized coordinate of the corresponding reference point. Given an input feature sequence  $X \in \mathbb{R}^{T_S \times C}$ , the output  $h_m \in \mathbb{R}^{T_S \times (C/M)}$  of the  $m$ -th ( $m \in \{1, 2, \dots, M\}$ ) head of a TDA module is computed by an weighted sum of a set of key elements sampled from  $X$ :

$$h_m = \sum_{k=1}^K a_{mqk} \mathbf{W}_m^V X(t_q + \Delta t_{mqk}), \quad (1)$$

where  $K$  is the number of sampling points,  $a_{mqk} \in [0, 1]$  is the normalized attention weight, and  $\Delta t_{mqk} \in [0, 1]$  is the sampling offset relative to  $t_q$ .  $X(t_q + \Delta t_{mqk})$  is the linear interpolated feature at  $t_q + \Delta t_{mqk}$  as it is fractional. Following [50], the attention weight  $a_{mqk}$  and the sampling offset  $\Delta t_{mqk}$  are predicted from the query feature  $z_q$  by linear projection. We normalize the attention weight with *softmax* to make  $\sum_{k=1}^K a_{mqk} = 1$ .  $\mathbf{W}_m^V \in \mathbb{R}^{C \times (C/M)}$  is a learnable weight. The output of TDA is computed by a linear combination of the outputs of different heads:

$$TDA(z_q, t_q, X) = \mathbf{W}^O \text{Concat}(h_1, h_2, \dots, h_m), \quad (2)$$

where  $\mathbf{W}^O \in \mathbb{R}^{C \times C}$  is a learnable weight.

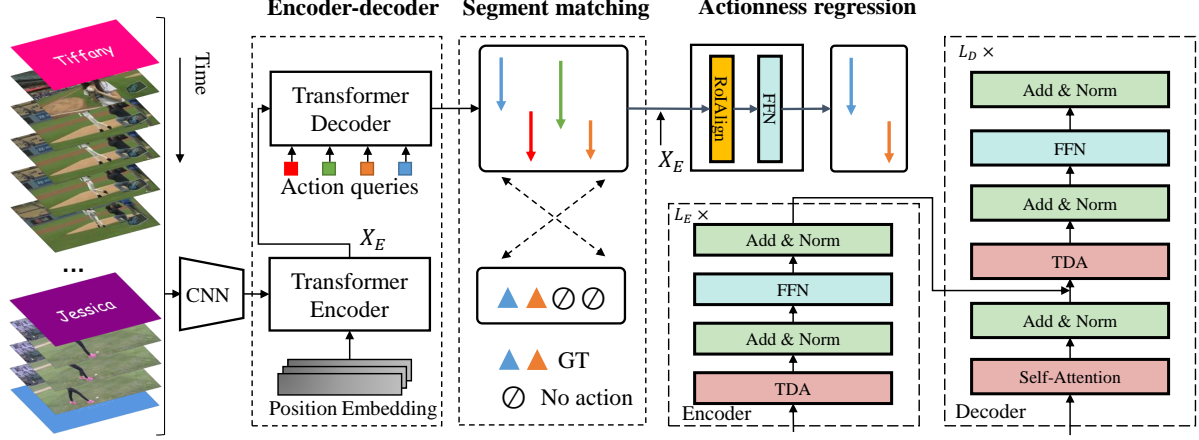


Figure 3. The architecture of TadTR. It takes the video features extracted with a CNN and position embedding as inputs and decodes a set of action predictions in parallel via a Transformer. The segment matching module determines a one-to-one ground truth assignment during training. The actionness regression head estimates the IoU with its best-matched ground truth for each prediction. The actionness score is used for ranking and filtering.

When computing the  $\tau$ -th frame in the output sequence, the query and the reference point are both the  $\tau$ -th frame in the input sequence. Therefore, we refer to TDA in the encoder as temporal deformable self-attention (TDSA). The query feature is the summation of the feature of that frame and the position embedding at that location. The position embedding is used to differentiate different locations in the input sequence. In this paper, we use the sinusoidal position embedding following [33]:

$$X_P(\tau, \gamma) = \begin{cases} \sin \frac{\tau}{10000^{\gamma/C}} & \gamma \text{ is even} \\ \cos \frac{\tau}{10000^{(\gamma-1)/C}} & \gamma \text{ is odd} \end{cases}. \quad (3)$$

**Decoder.** The decoder takes as inputs the encoder features  $X_E \in \mathbb{R}^{T_s \times C}$  and  $N_q$  action queries  $Q = \{q_i\}_{i=1}^{N_q}$  with learnable embeddings  $\{\hat{z}_{q_i}\}_{i=1}^{N_q}$  and transforms these embeddings to  $N_q$  action predictions  $\hat{Y} = \{\hat{y}_i\}$ . As illustrated in Fig. 3, the decoder consists of  $L_D$  sequential decoder layers. In each decoder layer, self-attention and temporal deformable cross-attention (TDCA) are both used. The self-attention module models the relation between action queries and updates their embeddings. The motivation here is that multiple actions in one video are often related. For example, a cricket shot action often appears after a cricket bowling action. To make an action prediction, each query needs to extract relevant context information from the video. To do that, we pass both the encoder features  $X_E$  and the query feature  $\hat{z}_{q_i} \in \mathbb{R}^C$  to the TDCA module. The output is formulated as  $TDA(\hat{z}_{q_i}, \hat{t}_{q_i}, X_E)$ . Here,  $\hat{t}_{q_i}$  is the coordinate of the reference point in  $X_E$ . It is predicted from the query embedding by a linear layer and normalized by *sigmoid* to make  $\hat{t}_{q_i} \in [0, 1]$ . The reference point can be seen as the initial estimation of the center of the corresponding action segment.

Different from TDSA in the encoder, the query embedding  $\hat{z}_{q_i}$  and the reference point is learnable. This allows the network to learn the global distribution of the action locations in the training dataset, which is more flexible than hand-crafted anchor setting or proposal sampling. An analysis is given in Sec. 4.4.

Based on the output of each decoder layer, we can apply two feed-forward networks to predict the classification probabilities  $\hat{p}_i$  and the temporal segment  $\hat{s}_i = (\hat{t}_i, \hat{d}_i)$  of the detection  $\hat{y}_i$  mapped from each query  $q_i$ .  $\hat{t}_i$  and  $\hat{d}_i$  are the coordinate of the center and the normalized length of the detection, respectively. To make the boundaries of the detection more accurate, a segment refinement is proposed, which is detailed below.

**Segment Refinement.** Transformer is able to capture long-range context information. However, the predicted action boundaries might be unsatisfactory for lack of locality. Therefore, we introduce a refinement mechanism to improve the localization performance. Based on the action segment  $\hat{s}_i^{(l)} = (\hat{t}_i^{(l)}, \hat{d}_i^{(l)})$  predicted by the  $l$ -th ( $1 \leq l \leq L_D - 1$ ) decoder layer, the  $(l+1)$ -th decoder layer refine its locations to make a new segment  $\hat{s}_i^{(l+1)} = (\hat{t}_i^{(l+1)}, \hat{d}_i^{(l+1)})$ :

$$\hat{t}_i^{(l+1)} = \sigma(\Delta t_i^{(l+1)} + \sigma^{-1}(\hat{t}_i^{(l)})) \quad (4)$$

$$\hat{d}_i^{(l+1)} = \sigma(\Delta d_i^{(l+1)} + \sigma^{-1}(\hat{d}_i^{(l)})), \quad (5)$$

where  $\hat{t}_i^{(l)}$  and  $\hat{d}_i^{(l)}$  are the coordinate of the center and the length of  $\hat{s}_i^{(l)}$ , respectively.  $\Delta t_i^{(l+1)}$  and  $\Delta d_i^{(l+1)}$  are the predicted offsets.  $\sigma(\cdot)$  and  $\sigma^{-1}(\cdot)$  are the sigmoid and the inverse sigmoid function, respectively. The center of the predicted segment at the  $l$ -th decoder layer is used as the reference point of the next decoder layer. In this way, the decoder learns to pay more attention to the locations around

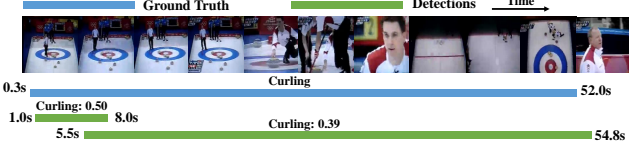


Figure 4. The Transformer may generate unreliable confidence scores. Here, a prediction with lower overlap with the curling action has a higher score than a more accurate prediction (0.50 vs. 0.39).

the estimated segment gradually, so that the boundaries can be more accurate.

**Actionness Regression.** One challenge of temporal action detection is the extreme scale (duration) variation of action instances, ranging from a few seconds to several minutes. Although the attention module can dynamically attend features in different ranges, it cannot always perfectly align the receptive field with the span of target actions. As a result, the classification score of the detections, predicted with *adaptive* context, may be unreliable for ranking. An example is shown in Fig. 4.

To mitigate this issue, we propose to regress the actionness of a detection with hindsight. We employ an actionness regression head that extracts context *aligned* with the interval of a predicted segment and predicts an actionness score upon it. Given the encoder feature sequence  $X_E$  and a predicted segment  $\hat{s}_i$  by the decoder, we first apply temporal RoIAlign [14] upon  $X_E$  to obtain the aligned features  $X_{s_i} \in \mathbb{R}^{T_R \times C}$  within the interval defined by  $s_i$  from  $X_E$ . Here,  $T_R$  is the number of bins for RoIAlign. As pointed out in previous works [46, 8, 9], the context information outside the segment is useful for assessing whether a segment is complete. Therefore, we slightly expand the segment by a factor of  $\epsilon$  when applying RoIAlign. The expanded segment can be expressed as  $(\hat{t}_i, \epsilon \hat{d}_i)$ . Then, a feed-forward network is used to predict the actionness score  $\hat{g}_i$  from the aligned feature.  $\hat{g}_i$  is supervised by the maximal IoU  $g_i$  (intersection over union) between  $s_i$  and all ground truth actions. In this way, the prediction with the highest IoU is expected to be ranked first among all predictions.

One may argue that the actionness regression head makes TadTR a two-stage detector. In fact, TadTR is significantly different from traditional two-stage methods. First, TadTR can already produce complete action detections without actionness regression. The actionness regression head is simply for more reliable confidence scores. In contrast, a two-stage detector is unable to make complete predictions without the second stage. Second, TadTR produces very sparse action predictions. It does require a preliminary stage to evaluate dense candidates as two-stage methods do. Therefore it requires low computation cost.

For convenience, we denote TadTR without actionness regression and segment refinement as *TadTR-base*.

## 3.2. Training and Inference

**Segment Matching.** The segment matching module determines the targets assigned to each detection during training. Inspired by DETR [6] in object detection, we frame it as a set-to-set bipartite matching problem and solve it with the Hungarian algorithm.

Let  $Y = \{y_j\}_{j=1}^{N_q}$  be a set of ground truth actions padded with  $\emptyset$  (no action) and  $\pi$  be the permutation that assigns each target  $y_j$  to the corresponding detection  $\hat{y}_{\pi(y_j)}$ . Bipartite matching aims to find a permutation that minimizes the overall matching cost:

$$\hat{\pi} = \arg \min \sum_{j=1}^{N_q} \mathcal{C}(y_j, \hat{y}_{\pi(j)}). \quad (6)$$

The matching cost considers the classification probabilities and the distance between ground truth and predicated segments. Specifically,  $\mathcal{C}(y_j, \hat{y}_{\pi(j)})$  is defined as

$$- \mathbb{1}_{c_j \neq \emptyset} [(\hat{p}_{\pi(j)}(c_j) + \mathcal{L}_{seg}(s_j, \hat{s}_{\pi(j)}))], \quad (7)$$

where  $c_j$  and  $s_j$  are the class label and the temporal segment of  $y_j$ .  $\mathcal{L}_{seg}(s_j, \hat{s}_{\pi(j)})$  is the distance between the predicted location and the ground truth location, defined as

$$\lambda_{iou} \mathcal{L}_{iou}(s_j, \hat{s}_{\pi(j)}) + \lambda_{coord} \mathcal{L}_{L1}(s_j, \hat{s}_{\pi(j)}), \quad (8)$$

where  $\mathcal{L}_{L1}$  is the  $L_1$  distance and  $\mathcal{L}_{iou}$  is the IoU loss. IoU loss is defined as the the opposite number of the IoU.  $\lambda_{iou}$  and  $\lambda_{coord}$  are hyper-parameters.

Through the set-based segment matching, each ground truth will be assigned to only one prediction, thus avoiding duplicate predictions. This brings two merits. First, TadTR does not rely on the non-differentiable non-maximal suppression (NMS) for post-processing and enjoys end-to-end training. Second, we can make sparse predictions with limited queries (*e.g.* 10) instead of dense predictions in many previous works (*e.g.* tens of thousands for BMN [16] and G-TAD [37]), which saves the computation cost.

In a way, the segment matching module performs a learnable NMS. The matching cost takes the classification scores of the detections into account. In this way, those detections with lower scores are more likely to be assigned with a non-action target. As a result, their classification scores will be suppressed in the training process.

**Loss Functions.** Once the ground truth assignment is determined, we optimize the network by minimizing the following multi-part loss functions:

$$\mathcal{L} = \sum_{j=1}^{N_q} [-\log \hat{p}_{\hat{\pi}(j)}(c_j) + \mathbb{1}_{c_j \neq \emptyset} \mathcal{L}_{seg}(s_j, \hat{s}_{\hat{\pi}(j)}) + \lambda_{act} \mathcal{L}_{L1}(\hat{g}_{\hat{\pi}(j)}, g_{\hat{\pi}(j)})], \quad (9)$$

where the first two items optimize the detections from the decoder and the last optimizes the outputs of actionness regression.  $\hat{\pi}$  is the solution of Equation 6.  $\lambda_{act}$  is a hyper-parameter.

**Inference.** During inference, we ignore the action predictions from all but the last decoder layer. The production of the actionness score and the classification probabilities predicted by the decoder is used for detection ranking.

## 4. Experiments

### 4.1. Experimental Setup

**Datasets and Evaluation Metrics.** We conduct experiments on THUMOS14 [15], HACS Segments [44], and ActivityNet-1.3 [5]. THUMOS14 is built on videos from 20 sports action classes. It contains 200 and 213 untrimmed videos for training and testing. There are 3007 and 3358 action instances on the two sets. ActivityNet-1.3 and HACS Segments share the same 200 classes of daily activities. Both datasets are split into three sets: training, validation, and testing. The numbers of videos in these sets are 10024, 4926, and 5044 respectively on ActivityNet-1.3, and 37613, 5981, and 5987 on HACS Segments. On both datasets, the annotations on the testing set are reserved by the organizers. Therefore, we evaluate on the validation set.

Following conventions, the mean average precision (mAP) at different IoU thresholds is used for performance evaluation. On THUMOS14, the IoU thresholds for computing mAPs are [0.3 : 0.7 : 0.1]. On the other two datasets, we report mAPs at the thresholds {0.5, 0.75, 0.95} and the average mAP at the thresholds [0.5 : 0.95 : 0.05].

**Video Feature Extraction.** Most TAD methods are based on offline extracted video features. For easier comparison with them, we also use video features as the input of our method. For experiments on HACS Segments, we directly use the official I3D features<sup>1</sup>, which are extracted with I3D trained on Kinetics at 2FPS. On the other datasets, we use the commonly used features in previous works. On THUMOS14, the two-stream I3D [7] networks pre-trained on Kinetics [7] are taken as the video encoder, and the features are extracted every 8 frames. On ActivityNet-1.3, we use the two-stream TSN [35] features extracted at 5FPS. Following previous works [16, 37], we resize the video features to a fixed length of 100 via linear interpolation on ActivityNet-1.3 and HACS Segments.

**Implementation Details.** The dimension of the feed-forward network is 2048.  $C$  is set to 256.  $L_E$  and  $L_D$  are set to 2 and 4, respectively. The loss weights  $\lambda_{iou}$ ,  $\lambda_{coord}$  and  $\lambda_{act}$  are set to 2, 5 and 5 respectively. The numbers of attention heads  $M$  and sampling points  $K$  are set

<sup>1</sup>[http://hacs.csail.mit.edu/hacs\\_segments\\_features.zip](http://hacs.csail.mit.edu/hacs_segments_features.zip)

to 8 and 4, respectively. The parameters of the linear layers that predict attention weights are initialized to zero. We initialize the linear layers that predict sampling offsets to make  $\{\Delta p_{mqk}\}_{m=1}^8 = (k, 0, -k, 0, k, 0, -k, 0)$  at initialization. The expanding factor  $\epsilon$  and the number of bins  $T_R$  for RoIAlign in the actionness regression head are 1.5 and 16 respectively.

TadTR is trained using AdamW [23] optimizer. The initial learning rate is  $2 \times 10^{-4}$  and scaled by a factor of 0.1 after training for a certain number of epochs. The learning rates of the linear projection layers for predicting attention weights and sampling offsets are multiplied by 0.1. We train the models for 30, 15, and 20 epochs and decrease the learning rate after 25, 12, and 15 epochs on THUMOS14, ActivityNet-1.3, and HACS Segments respectively. The batch size is set to 16.

The experiments are conducted on a workstation with a single Tesla P100 GPU card, and Intel(R) Xeon(R) CPU E5-2682 v4 @ 2.50GHz. It takes around 40 minutes, 1.5 hours, and 7 hours to finish training on THUMOS14, ActivityNet-1.3, and HACS Segments, respectively.

### 4.2. Main Results

**THUMOS14.** Table 1 demonstrates the temporal action detection performance and run time comparison on the testing set of THUMOS14. We measure the run time of these methods with publicly available implementations under the same environment (a single P100 GPU). We run methods on the full testing set with batch size set to 1 and report the average time and FLOPs per video. The average length of videos on THUMOS14 is 217 seconds. BMN [16] and G-TAD [37] use two-stream TSN [35] features originally. For fair comparison, we also report their performance with I3D features. We observe that:

- 1) Compared with previous methods, TadTR achieves the best performance in terms of average mAP.
- 2) Compared with the strongest single-network method A2Net [38], TadTR runs  $10\times$  faster with 5.0% higher average mAP. A2Net is slow due to the heavy network and a large number of anchors.
- 3) Compared with the second best method P-GCN [43], TadTR achieves slightly better performance with  $46\times$  faster inference speed. We note that P-GCN has relatively lower FLOPs than other methods, as it contains no 1D convolution layers for temporal modelling. However, the graph structure restricts its speed. It needs to extract the features of extra 24 neighboring proposals to compute the detection score of a proposal.
- 4) The performance of TadTR can be further boosted when it is combined with P-GCN. Specifically, we pass the detections from TadTR as proposals to the proposal classification stage of P-GCN and use the detection scores by P-GCN. Notably, TadTR achieves an mAP of 54.1% at

Table 1. Comparison with state-of-the-art methods on THUMOS14. Run time is the average inference time per video, including post-processing operations, such as NMS. For proposal generation methods (BSN, MGG, BMN, G-TAD, MR, BC-GNN) in the first group, the run time of the classification stage is not included as the classification models are not available. E2E: end-to-end. TS: two-stream. \* Results copied from [38]. \*\* Our implementation.

Method	Feature	Single-network	E2E	0.3	0.4	0.5	0.6	0.7	Avg.	Run time (ms)	FLOPs (G)
Yeung <i>et al.</i> [39]	VGG16	✓	✓	36.0	26.4	17.1	-	-	-	195	3.9
Yuan <i>et al.</i> [42]	TS	-	-	36.5	27.8	17.8	-	-	-	-	-
SSAD [17]	TS	✓	-	43.0	35.0	24.6	-	-	-	-	-
R-C3D [36]	C3D	✓	-	44.8	35.6	28.9	-	-	-	-	-
SSN [47]	TS	-	-	51.9	41.0	29.8	-	-	-	-	-
TAL-Net [8]	I3D	✓	-	53.2	48.5	42.8	33.8	20.8	39.8	-	-
BSN [18]	TS	-	-	53.5	45.0	36.9	28.4	20.0	36.8	2065	3.4
MGG [21]	TS	-	-	53.9	46.8	37.4	29.5	21.3	37.8	-	-
BMN [16]	TS	-	-	56.0	47.4	38.8	29.7	20.5	38.5	483	171.0
BC-GNN [11]	TS	-	-	57.1	49.1	40.4	31.2	23.1	40.2	-	-
G-TAD [37]	TS	-	-	54.5	47.6	40.2	30.8	23.4	39.3	4440	639.8
BMN* (I3D) [16]	I3D	-	-	56.4	47.9	39.2	30.2	21.2	39.0	-	-
G-TAD** (I3D) [37]	I3D	-	-	58.7	52.7	44.9	33.6	23.8	42.7	3552	368.9
MR [45]	I3D	-	-	53.9	50.7	45.4	38.0	28.5	43.3	644	36.8
A2Net [38]	I3D	✓	-	58.6	54.1	45.5	32.5	17.2	41.6	1554	30.4
P-GCN [43]	I3D	-	-	63.6	57.8	49.1	-	-	-	7298	4.4
P-GCN** [43]	I3D	-	-	64.9	59.0	49.4	36.7	22.6	46.5	7298	4.4
TadTR (Ours)	I3D	✓	✓	62.4	57.4	49.2	37.8	26.3	46.6	<b>155</b>	<b>0.75</b>
TadTR+P-GCN (Ours)	I3D	-	-	<b>70.8</b>	<b>63.5</b>	<b>54.1</b>	<b>41.7</b>	28.0	<b>51.6</b>	1647	1.0

IoU=0.5, which is 5.1% higher than primitive P-GCN. The result reveals the great potential of TadTR. As for run time, TadTR+P-GCN is much faster than primitive P-GCN, as it has fewer detections than its original proposal generator.

The above results indicate that TadTR is both accurate and efficient. We also note that many other methods are composed of multiple networks for different functions, while TadTR is able to perform action detection with only a *single* unified network.

We note that our method is not directly comparable with [39], since it is a very early work and uses different features. The goal of this paper is not to compete against it. Instead, we aim to explore an alternative end-to-end framework with adaptive context and validate whether it can achieve competitive performance over more complicated and well optimized methods. The computation cost of TadTR is also not comparable with those methods that directly take image as input, such as R-C3D. Most previous works use video features as input and focus on the design of detection network.

**HACS Segments.** This is a recently introduced dataset, therefore the results of many early methods on this dataset are not available. We report the performance of TadTR, SSN [46], and the state-of-the-art method G-TAD [37] in Table 2. Our method achieves an average mAP of 30.83%, which clearly outperforms SSN (+11.86% mAP) and G-TAD (+3.35% mAP). Besides, our method requires 455× less computation cost than G-TAD. As for run time, the network inference and post-processing step of G-TAD take 33

ms and 908 ms per video, respectively. The total run time is 941 ms, 49.5× that of TadTR (19 ms). The results again illustrate the superiority of TadTR.

**ActivityNet-1.3.** In Table 3, we compare temporal action detection performance of different methods on the validation set of ActivityNet-1.3. Some methods, such as G-TAD, only implement action proposal generation and cannot produce action detections without external action classifiers. We divide the methods into two groups according to whether external action classifiers are used. Being simple and end-to-end trainable, TadTR achieves an average mAP of 27.75%, which is stronger than more complicated methods such as TAL-Net [8] and P-GCN [43]. Compared with the previous best single-network detector TAL-Net, we improve the performance by 7.53%.

To enhance the detection performance, we also try combining TadTR with an ensemble of action classifiers trained by [47] following previous works [38, 37]. To be concrete, we pass the detections by TadTR to the classifiers and fuse the classification scores of TadTR and the classifiers by multiplication. When fused with [46], TadTR enjoys a significant performance boost to an average mAP of 32.27%. The results are better than recent methods such as MR [45] and A2Net [38] that are also combined with [47].

To make a comparison with highly optimized two-stage methods, such as BMN [16] and G-TAD [37], we also develop a two-stage variant TadTR+BMN. This is implemented by combining the encoder of TadTR and the detection head of BMN. Owing to the adaptive context captured

Table 2. Comparison of different methods and different variants of TadTR on the validation set of HACS Segments. The results of SSN are from [44].

Method	0.5	0.75	0.95	Avg.	FLOPs (M)
SSN [47]	28.82	18.80	5.32	18.97	-
G-TAD [37]	41.08	27.59	8.34	27.48	45725.9
<b>Ours</b>					
TadTR	<b>45.16</b>	<b>30.70</b>	<b>11.78</b>	<b>30.83</b>	100.5
TadTR w/o encoder	39.65	26.99	9.08	26.94	95.3
TadTR w/o instance-level context	43.11	29.97	10.43	29.70	66.8
TadTR with a 1D CNN encoder	40.96	28.00	9.73	27.95	134.8
TadTR with dense attention	22.76	12.52	4.19	13.58	564.5
TadTR w/o actionness regression	42.10	28.44	10.23	28.51	99.4
TadTR w/o segment refinement	39.89	28.03	9.54	27.65	99.8

by the Transformer encoder, TadTR+BMN achieves an improvement of 0.7% over BMN, reaching 34.55% average mAP. It also outperforms the recent method G-TAD. This indicates the great potential of Transformer in temporal action detection. The result is also much higher than vanilla TadTR. We conjecture that the performance bottleneck in ActivityNet is the confidence prediction of detections. Two-stage methods have orders of magnitude more candidates, providing sufficient training samples for the confidence prediction head. In the future, we plan to investigate better strategies to train the confidence prediction head of TadTR.

### 4.3. Ablation Study

**The importance of context information.** The key of Transformer is the self-attention mechanism that incorporates the context in a video sequence. In TadTR, we leverage two kinds of context, inter-snippet context from all snippets and inter-action context from all action queries, which are captured by Transformer encoder and the self-attention module in Transformer decoder respectively. By removing Transformer encoder, we get a variant “TadTR w/o encoder”. By removing the self-attention module in the decoder, we get a variant “TadTR w/o inter-action context”. We report the performance of the two variants in Table 2. It is observed that removing the encoder leads to a significant performance drop of 3.93% average mAP. It indicates that the Transformer encoder is crucial for our model, as the decoder requires long-range and adaptive context to reason the relations between the actions and the video. Removing instance-level context, the average mAP drops by 1.13%. We conclude that the context information from other action instances is also helpful for action detection.

**Transformer encoder v.s. CNN encoder.** We try replacing the Transformer encoder with a 1D CNN encoder, which is common for temporal modeling in previous TAD methods. The 1D CNN encoder is composed of two 1D convolutional layers with 256 filters of kernel size 3 and ReLU activation. This variant is denoted as “TadTR with a 1D CNN

encoder”. As can be observed in Table 2, the performance of this variant is worse than TadTR (-2.92% average mAP), even with higher computation cost. We also explore deeper CNNs and larger convolution kernels, but no improvement is observed. The results show that 1D CNN is inferior to Transformer encoder.

**Dense attention v.s. temporal deformable attention.** We try replacing all temporal deformable attention modules in TadTR with vanilla dense attention modules. This variant is called “TadTR with dense attention”. As depicted in Table 2, the performance of this variant is far behind TadTR (13.58% v.s. 30.83% average mAP). Besides, it has  $5.7\times$  higher computation cost than that of TadTR. The main reason is that the dense attention lacks induced bias. A dense attention module is initialized to nearly take an average of all locations in the input sequence approximately. It is hard to learn to focus on specific locations. Therefore, temporal deformable attention is a better choice.

**Effects of actionness regression and segment refinement.** We study the effects of iterative segment refinement and actionness regression by removing them from TadTR individually, resulting in 2 different model variants. Their results on HACS Segments are presented in Table 2. Comparing TadTR w/o actionness regression and TadTR, we observe that actionness regression leads to improvements of all metrics. Specifically, the improvements are 3.06%, 2.26%, 1.55%, and 2.32% in terms of mAP at IoU 0.5, 0.75, 0.95 and the average mAP. Several qualitative examples are presented in Fig. 5 to show how actionness regression helps. It is able to produce more reliable confidence scores for the action predictions by Transformer, owing to explicit feature alignment. Comparing TadTR w/o segment refinement and TadTR, we find this component helpful for improving the localization accuracy. It improves the mAP at the strict threshold of 0.95 by a large margin of 2.24%. The mAPs at other thresholds are also consistently improved.

Besides the detection performance, another important aspect is the computation cost of the detector. In terms of



Table 3. Comparison of different methods on ActivityNet-1.3. Methods in the second group are combined with an ensemble of action classifiers [47]. The computation costs (in FLOPs) of the action classifiers are not included.

Method	Single-network	E2E	0.5	0.75	0.95	Avg.	FLOPs (G)
<b>Self-contained methods</b>							
CDC [29]	-	-	43.83	25.88	0.21	22.77	-
R-C3D [36]	✓	-	26.8	-	-	-	-
SSN [46]	-	-	39.12	23.48	5.49	23.98	-
TAL-Net [8]	✓	-	38.23	18.30	1.30	20.22	-
P-GCN [43]	-	-	42.90	28.14	2.47	26.99	5.0
TadTR (Ours)	✓	✓	<b>40.85</b>	<b>28.44</b>	<b>7.84</b>	<b>27.75</b>	<b>0.038</b>
<b>Combined with an ensemble of action classifiers [47]</b>							
P-GCN [43]	-	-	48.26	33.16	3.27	31.11	5.0
MR [45]	-	-	43.47	33.91	<b>9.21</b>	30.12	-
A2Net [38]	-	-	43.55	28.69	3.70	27.75	1.2
BMN [16]	-	-	50.07	34.78	8.29	33.85	45.6
G-TAD [37]	-	-	50.36	34.60	9.02	34.09	45.7
TadTR (Ours)	-	-	49.08	32.58	8.49	32.27	<b>0.038</b>
TadTR+BMN (Ours)	-	-	<b>50.51</b>	<b>35.35</b>	8.18	<b>34.55</b>	45.6

Table 4. Effect of numbers of encoder layers and decoder layers. The detection performance is evaluated on HACS Segments.

$L_E$	$L_D$	0.5	0.75	0.95	Avg.	FLOPs (M)
2	4	<b>45.16</b>	<b>30.70</b>	<b>11.78</b>	<b>30.83</b>	<b>100.5</b>
4	4	44.63	30.39	10.76	30.39	105.6
6	4	40.55	27.55	9.88	27.63	110.8
2	2	42.10	29.05	9.57	28.84	<b>79.6</b>
2	4	<b>45.16</b>	<b>30.70</b>	<b>11.78</b>	<b>30.83</b>	100.5
2	6	45.20	30.82	10.67	30.74	121.3

FLOPs, adding or removing the two components has little impact, which is shown in Table 2. In terms of run time, we keep the same environment used in Fig. 1 and Table 1 for run time measurement. The average time cost per video is 130 ms for TadTR-base. Adding the rescoring module will increase the average time cost to 141 ms. With segment refinement enabled, the average time cost per video becomes 155 ms, which is still very efficient compared with state-of-the-art methods.

**Effects of the number of action queries.** Table 5 compares the performance of TadTR using different number of action queries ( $N_q$ ). The best performance is achieved at  $N_q = 40$  on THUMOS14,  $N_q = 30$  on HACS Segments and  $N_q = 10$  on ActivityNet-1.3. The results are reasonable, as the average number of action instances per video on THUMOS14 (15.4) is larger than that on ActivityNet-1.3 (1.5) and HACS Segments (2.8). We note that TadTR also achieves strong performance on other choices of  $N_q$ . Adjusting  $N_q$  is also much easier than manually setting a series of anchor scales in traditional methods.

**Effects of the numbers of encoder layers and decoder layers.** We evaluate TadTR with different numbers of en-

Table 5. Effect of the number of action queries on different datasets. The average mAPs are reported.

# queries	10	20	30	40	50
THUMOS14	43.52	45.27	45.75	<b>46.63</b>	45.49
HACS Segments	29.63	30.73	<b>30.83</b>	29.99	-
ActivityNet-1.3	<b>27.75</b>	26.47	26.27	26.29	-

Table 6. Impact of the number of sampling points  $K$  on the performance and computation cost on HACS Segments. The models are trained for half of the full training cycle (15 epochs).

# points	0.5	0.75	0.95	Avg.	FLOPs (M)
1	39.22	27.07	9.80	27.03	<b>99.1</b>
2	40.22	27.62	10.15	27.61	99.6
4	<b>41.20</b>	<b>28.52</b>	<b>10.63</b>	<b>28.49</b>	100.5
8	39.77	27.15	9.86	27.20	102.4

coder layers ( $L_E$ ) and decoder layers ( $L_D$ ) and report results in Table 4. With  $L_D$  fixed, the best performance is achieved when  $L_E$  is 2. Larger  $L_E$  gives inferior results probably due to the difficulty of training. Therefore, we set  $L_E$  to 2. With  $L_E$  fixed, the average mAP increases by 2.03% when  $L_D$  increases from 2 to 4. Larger  $L_D$  gives a slightly lower performance. Therefore we suggest setting  $L_D$  to 4.

**Effect of the number of sampling points.** Table 6 compares the performance and computation cost using different numbers of sampling points  $K$  in TDA modules on HACS Segments. We observe that moderately increasing  $K$  improves the performance, as more temporal details can be captured. The best performance is achieved at  $K = 4$ . The number of sampling points has little impact on the computation cost.

**Effect of the number of attention heads.** Table 7 com-

Table 7. Effect of the number of attention heads  $M$  on the performance and computation cost on HACS Segments. The models are trained for half of the full training cycle (15 epochs).

# head	0.5	0.75	0.95	Avg.	FLOPs (M)
1	38.62	25.25	7.94	25.57	<b>100.2</b>
2	40.30	26.37	8.09	26.52	100.2
4	40.74	28.41	10.51	28.30	100.3
8	<b>41.20</b>	<b>28.52</b>	<b>10.63</b>	<b>28.49</b>	100.5
16	41.07	28.35	10.23	28.31	100.9

compares the performance and computation cost using different number of attention heads  $M$  on HACS Segments. It is observed that that moderately increasing  $M$  boosts the performance, as more diverse features can be learned. The performance is saturated at  $M = 8$ . Similar to the number of sampling points, the number of attention heads has little impact on the computation cost.

#### 4.4. Analysis

**Visualization of action queries.** Fig. 6 illustrates the distribution of locations and scales (lengths) of output actions associated with each action query. We observe that each query produces action predictions in certain locations and scales. Different locations and scales are covered by a small number of queries. It means that the detector learns the distribution of actions in the training dataset. This is more flexible and efficient than the handcrafted anchor design in previous methods.

**Visualization of attention.** Fig. 7 visualizes attention of the last encoder layer and the last decoder layer. We use different colors to distinguish different attention heads. We observe that: (1) Different attention heads focus on different temporal regions and scales. The red and the pink points are sparsely distributed on the left side of a reference point. The blue and the purple points are sparsely distributed on the right. Other points are near the referent points. (2) Sampling points in the decoder almost cover the same temporal extent of an action prediction, providing a very large receptive field. Differently, sampling points in the encoder have a more flexible distribution, capturing a moderate amount of context.

## 5. Conclusion

We propose TadTR, a simple end-to-end framework for temporal action detection based on Transformer. It views the TAD task as a direct set-prediction problem and maps a series of learnable embeddings to action instances in parallel by adaptively extracting temporal context in the video. It simplifies the pipeline of TAD and removes hand-crafted designs such as anchor setting and post-processing. Extensive experiments are conducted to validate the performance and efficiency of TadTR and the effectiveness of different

components. TadTR achieves state-of-the-art or competitive performance on HACS Segments, THUMOS14, and ActivityNet-1.3 with significantly lower computation costs. We hope that our work could trigger the development of efficient models and vision Transformers for temporal action detection.

## References

- [1] Yueran Bai, Yingying Wang, Yunhai Tong, Yang Yang, Qiyue Liu, and Junhui Liu. Boundary content graph neural network for temporal action proposal generation. In *ECCV*, pages 121–137, 2020.
- [2] Gedas Bertasius, Heng Wang, and Lorenzo Torresani. Is space-time attention all you need for video understanding? In *ICML*, July 2021.
- [3] Shyamal Buch, Victor Escorcia, Chuanqi Shen, Bernard Ghanem, and Juan Carlos Niebles. Sst: Single-stream temporal action proposals. In *CVPR*, pages 6373–6382, 2017.
- [4] Fabian Caba Heilbron, Juan Carlos Niebles, and Bernard Ghanem. Fast temporal activity proposals for efficient detection of human actions in untrimmed videos. In *CVPR*, pages 1914–1923, 2016.
- [5] Fabian Caba Heilbron, Victor Escorcia, Bernard Ghanem, and Juan Carlos Niebles. Activitynet: A large-scale video benchmark for human activity understanding. In *CVPR*, pages 961–970, 2015.
- [6] Nicolas Carion, Francisco Massa, Gabriel Synnaeve, Nicolas Usunier, Alexander Kirillov, and Sergey Zagoruyko. End-to-end object detection with transformers. In *ECCV*, pages 213–229, 2020.
- [7] Joao Carreira and Andrew Zisserman. Quo vadis, action recognition? a new model and the kinetics dataset. In *CVPR*, pages 4724–4733, 2017.
- [8] Yu-Wei Chao, Sudheendra Vijayanarasimhan, Bryan Seybold, David A Ross, Jia Deng, and Rahul Sukthankar. Re-thinking the faster r-cnn architecture for temporal action localization. In *CVPR*, pages 1130–1139, 2018.
- [9] Xiyang Dai, Bharat Singh, Guyue Zhang, Larry S Davis, and Yan Qiu Chen. Temporal context network for activity localization in videos. In *ICCV*, pages 5727–5736, 2017.
- [10] Victor Escorcia, Fabian Caba Heilbron, Juan Carlos Niebles, and Bernard Ghanem. Daps: Deep action proposals for action understanding. In *ECCV*, pages 768–784, 2016.
- [11] Jiyang Gao, Kan Chen, and Ram Nevatia. Ctap: Complementary temporal action proposal generation. In *ECCV*, September 2018.
- [12] Jiyang Gao, Zhenheng Yang, Chen Sun, Kan Chen, and Ram Nevatia. Turn tap: Temporal unit regression network for temporal action proposals. In *ICCV*, pages 3648–3656, 2017.
- [13] Rohit Girdhar, Joao Carreira, Carl Doersch, and Andrew Zisserman. Video action transformer network. In *CVPR*, pages 244–253, 2019.
- [14] Kaiming He, Georgia Gkioxari, Piotr Dollár, and Ross Girshick. Mask r-cnn. In *ICCV*, pages 2961–2969, 2017.
- [15] YG Jiang, Jingen Liu, A Roshan Zamir, G Toderici, I Laptev, Mubarak Shah, and Rahul Sukthankar. Thumos challenge: Action recognition with a large number of classes, 2014.

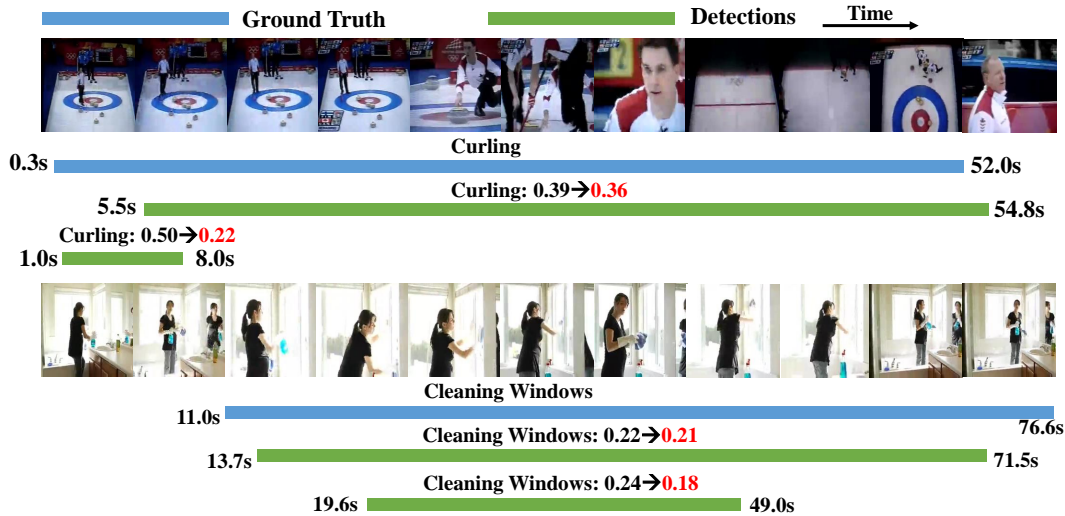


Figure 5. actionness regression improves the ranking of detections. In each of the above cases, the more accurate obtains a lower score than the less accurate one before rescoring. With the new scores (red color) applied, the ranking order turns satisfactory.

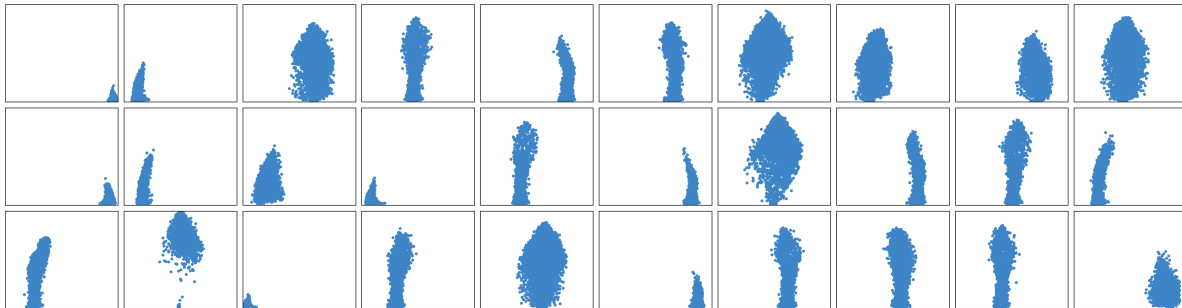
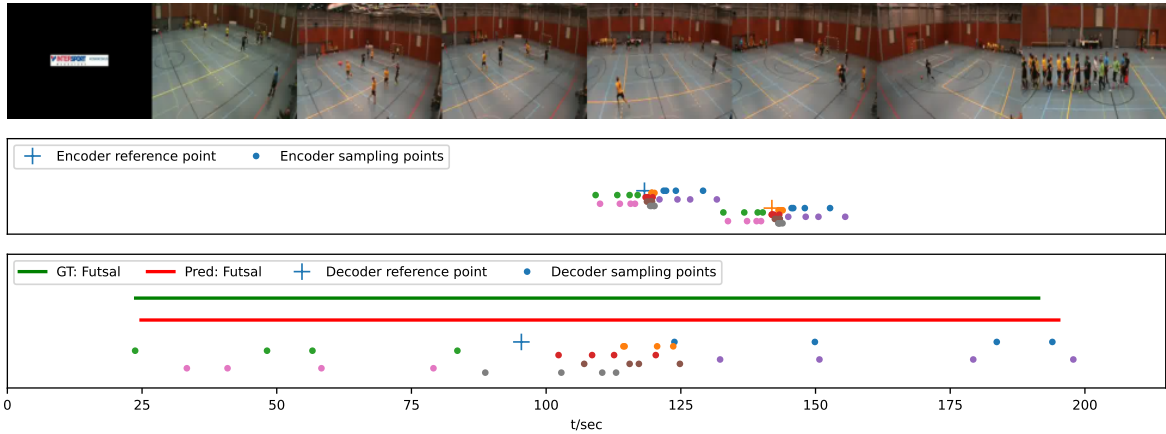
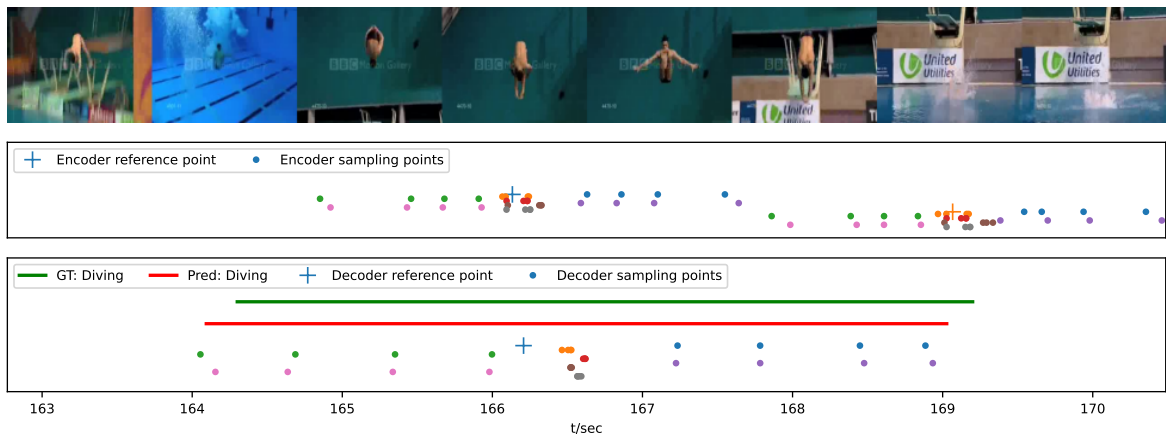


Figure 6. Distribution of all output actions on all videos from HACS Segments validation set for 30 query slots with action queries. In each 1-by-1 square, an action prediction predicted from the corresponding action query is represented as a point, and the horizontal and vertical coordinates are the coordinate of the center and the length normalized by the video length. For example, we observe that the first and the second queries are responsible for actions near the ending of a video and actions near the starting of a video, respectively.

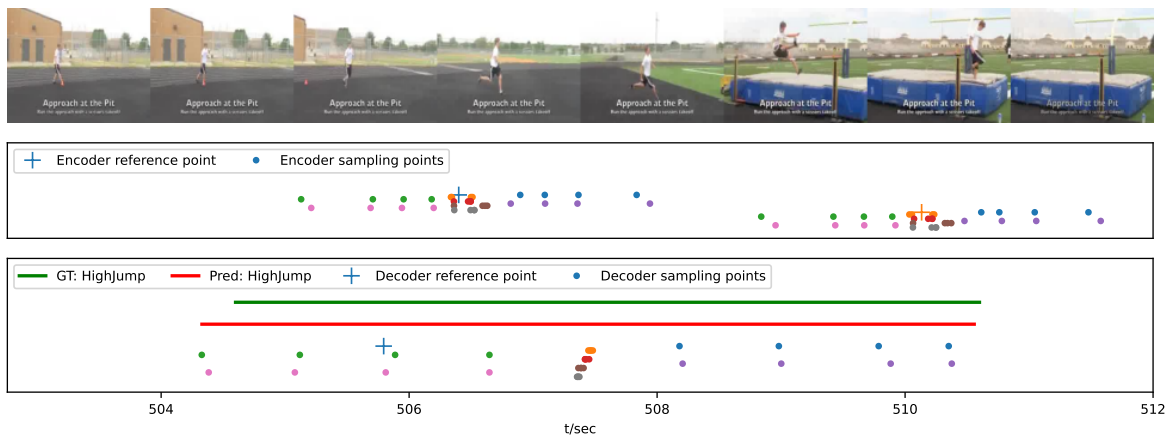
- [16] Tianwei Lin, Xiao Liu, Xin Li, Errui Ding, and Shilei Wen. Bmn: Boundary-matching network for temporal action proposal generation. In *ICCV*, pages 3889–3898, 2019.
- [17] Tianwei Lin, Xu Zhao, and Zheng Shou. Single shot temporal action detection. In *ACM MM*, pages 988–996, 2017.
- [18] Tianwei Lin, Xu Zhao, Haisheng Su, Chongjing Wang, and Ming Yang. Bsn: Boundary sensitive network for temporal action proposal generation. In *ECCV*, September 2018.
- [19] Daochang Liu, Tingting Jiang, and Yizhou Wang. Completeness modeling and context separation for weakly supervised temporal action localization. In *CVPR*, pages 1298–1307, 2019.
- [20] Xiaolong Liu, Yao Hu, Song Bai, Fei Ding, Xiang Bai, and Philip H. S. Torr. Multi-shot temporal event localization: A benchmark. In *CVPR*, pages 12596–12606, June 2021.
- [21] Yuan Liu, Lin Ma, Yifeng Zhang, Wei Liu, and Shih-Fu Chang. Multi-granularity generator for temporal action proposal. In *CVPR*, pages 3604–3613, 2019.
- [22] Fuchen Long, Ting Yao, Zhaofan Qiu, Xinmei Tian, Jiebo Luo, and Tao Mei. Gaussian temporal awareness networks for action localization. In *CVPR*, pages 344–353, 2019.
- [23] Ilya Loshchilov and Frank Hutter. Decoupled weight decay regularization. In *ICLR*, 2017.
- [24] Fan Ma, Linchao Zhu, Yi Yang, Shengxin Zha, Gourab Kundu, Matt Feiszli, and Zheng Shou. Sf-net: Single-frame supervision for temporal action localization. In *ECCV*, pages 420–437. Springer, 2020.
- [25] Shugao Ma, Leonid Sigal, and Stan Sclaroff. Learning activity progression in lstms for activity detection and early detection. In *CVPR*, June 2016.
- [26] Phuc Nguyen, Ting Liu, Gautam Prasad, and Bohyung Han. Weakly supervised action localization by sparse temporal pooling network. In *CVPR*, pages 6752–6761, 2018.
- [27] Sujoy Paul, Surya Roy, and Amit K. Roy-Chowdhury. W-talc: Weakly-supervised temporal activity localization and classification. In *ECCV*, September 2018.
- [28] Alexander Richard and Juergen Gall. Temporal action detection using a statistical language model. In *CVPR*, pages 3131–3140, 2016.
- [29] Zheng Shou, Jonathan Chan, Alireza Zareian, Kazuyuki Miyazawa, and Shih-Fu Chang. Cdc: Convolutional-de-



(a) Futsal



(b) Diving



(c) High jump

Figure 7. Visualization of attention. Each subfigure is composed of three rows. The first row is uniformly sampled video frames. The second row visualizes the attention at two randomly picked reference points in the last encoder layer. The third row visualizes the attention for the predicted action in the last decoder layer. Sampling points in different attention heads are in different colors. We separate the sampling points in different heads vertically for better readability. Best viewed in color.

- convolutional networks for precise temporal action localization in untrimmed videos. In *ICCV*, pages 1417–1426, 2017.
- [30] Zheng Shou, Hang Gao, Lei Zhang, Kazuyuki Miyazawa, and Shih-Fu Chang. Autoloc: Weakly-supervised temporal action localization in untrimmed videos. In *ECCV*, pages 154–171, 2018.
- [31] Zheng Shou, Dongang Wang, and Shih-Fu Chang. Temporal action localization in untrimmed videos via multi-stage cnns. In *CVPR*, pages 1049–1058, 2016.
- [32] Chen Sun, Austin Myers, Carl Vondrick, Kevin Murphy, and Cordelia Schmid. Videobert: A joint model for video and language representation learning. In *ICCV*, pages 7464–7473, 2019.
- [33] Ashish Vaswani, Noam Shazeer, Niki Parmar, Jakob Uszkoreit, Llion Jones, Aidan N. Gomez, Lukasz Kaiser, and Illia Polosukhin. Attention is all you need. In *NIPS*, pages 5998–6008, 2017.
- [34] Limin Wang, Yuanjun Xiong, Dahua Lin, and Luc Van Gool. Untrimmednets for weakly supervised action recognition and detection. In *CVPR*, pages 4325–4334, 2017.
- [35] Limin Wang, Yuanjun Xiong, Zhe Wang, Yu Qiao, Dahua Lin, Xiaoou Tang, and Luc Van Gool. Temporal segment networks: Towards good practices for deep action recognition. In *ECCV*, pages 20–36, 2016.
- [36] Huijuan Xu, Abir Das, and Kate Saenko. R-c3d: region convolutional 3d network for temporal activity detection. In *ICCV*, pages 5794–5803, 2017.
- [37] Mengmeng Xu, Chen Zhao, David S Rojas, Ali Thabet, and Bernard Ghanem. G-TAD: Sub-graph localization for temporal action detection. In *CVPR*, pages 10156–10165, 2020.
- [38] Le Yang, Houwen Peng, Dingwen Zhang, Jianlong Fu, and Junwei Han. Revisiting anchor mechanisms for temporal action localization. *IEEE Transactions on Image Processing*, 29:8535–8548, 2020.
- [39] Serena Yeung, Olga Russakovsky, Greg Mori, and Li Fei-Fei. End-to-end learning of action detection from frame glimpses in videos. In *CVPR*, pages 2678–2687, 2016.
- [40] Tan Yu, Zhou Ren, Yuncheng Li, Enxu Yan, Ning Xu, and Junsong Yuan. Temporal structure mining for weakly supervised action detection. In *ICCV*, pages 5522–5531, 2019.
- [41] Jun Yuan, Bingbing Ni, Xiaokang Yang, and Ashraf A Kassim. Temporal action localization with pyramid of score distribution features. In *CVPR*, pages 3093–3102, 2016.
- [42] Ze-Huan Yuan, Jonathan C Stroud, Tong Lu, and Jia Deng. Temporal action localization by structured maximal sums. In *CVPR*, volume 2, page 7, 2017.
- [43] Runhao Zeng, Wenbing Huang, Mingkui Tan, Yu Rong, Peilin Zhao, Junzhou Huang, and Chuang Gan. Graph convolutional networks for temporal action localization. In *ICCV*, pages 7094–7103, 2019.
- [44] Hang Zhao, Antonio Torralba, Lorenzo Torresani, and Zhicheng Yan. HACS: human action clips and segments dataset for recognition and temporal localization. In *ICCV*, pages 8667–8677, 2019.
- [45] Peisen Zhao, Lingxi Xie, Chen Ju, Ya Zhang, Yanfeng Wang, and Qi Tian. Bottom-up temporal action localization with mutual regularization. In *ECCV*, 2020.
- [46] Yue Zhao, Yuanjun Xiong, Limin Wang, Zhirong Wu, Xiaoou Tang, and Dahua Lin. Temporal action detection with structured segment networks. *ICCV*, pages 2914–2923, 2017.
- [47] Yue Zhao, Bowen Zhang, Zhirong Wu, Shuo Yang, Lei Zhou, Sijie Yan, Limin Wang, Yuanjun Xiong, Wang Yali, Dahua Lin, Yu Qiao, and Xiaoou Tang. CUHK & ETHZ & SIAT submission to ActivityNet challenge 2017. *arXiv preprint arXiv:1710.08011*, pages 20–24, 2017.
- [48] Luowei Zhou, Yingbo Zhou, Jason J Corso, Richard Socher, and Caiming Xiong. End-to-end dense video captioning with masked transformer. In *CVPR*, pages 8739–8748, 2018.
- [49] Linchao Zhu and Yi Yang. Actbert: Learning global-local video-text representations. In *CVPR*, pages 8746–8755, 2020.
- [50] Xizhou Zhu, Weijie Su, Lewei Lu, Bin Li, Xiaogang Wang, and Jifeng Dai. Deformable detr: Deformable transformers for end-to-end object detection. In *ICLR*, 2021.